



OPEN

SUBJECT AREAS:
ELECTRONIC PROPERTIES
AND MATERIALS
ELECTRONIC DEVICES
IMAGING TECHNIQUES

Received
5 November 2013

Accepted
10 February 2014

Published
26 February 2014

Correspondence and
requests for materials
should be addressed to
C.M. (cmaragliano@
masdar.ac.ae)

Quantifying charge carrier concentration in ZnO thin films by Scanning Kelvin Probe Microscopy

C. Maragliano¹, S. Lilliu², M. S. Dahlem², M. Chiesa¹, T. Souier¹ & M. Stefancich¹

¹Institute Center for Energy (iEnergy), Masdar Institute of Science and Technology, Abu Dhabi, UAE, ²Institute Center for Microsystems (iMicro), Masdar Institute of Science and Technology, Abu Dhabi, UAE.

In the last years there has been a renewed interest for zinc oxide semiconductor, mainly triggered by its prospects in optoelectronic applications. In particular, zinc oxide thin films are being widely used for photovoltaic applications, in which the determination of the electrical conductivity is of great importance. Being an intrinsically doped material, the quantification of its doping concentration has always been challenging. Here we show how to probe the charge carrier density of zinc oxide thin films by Scanning Kelvin Probe Microscopy, a technique that allows measuring the contact potential difference between the tip and the sample surface with high spatial resolution. A simple electronic energy model is used for correlating the contact potential difference with the doping concentration in the material. Limitations of this technique are discussed in details and some experimental solutions are proposed. Two-dimensional doping concentration images acquired on radio frequency-sputtered intrinsic zinc oxide thin films with different thickness and deposited under different conditions are reported. We show that results inferred with this technique are in accordance with carrier concentration expected for zinc oxide thin films deposited under different conditions and obtained from resistivity and mobility measurements.

In the last century, Zinc Oxide (ZnO) attracted interest within the scientific community. Defined as the *future material*, ZnO has been widely studied since 1935. Lately a renewed interest for this material had risen. This is mainly due to reports of *p*-type conduction¹, ferromagnetic behavior² and improvements in epitaxial growth technologies that make this material suitable for the fabrication of optoelectronic³, piezoelectric⁴ and spintronic devices⁵. Extensive reviews on ZnO applications are available in the literature^{6,7}. Nano-crystalline ZnO thin films are being widely studied, especially for photovoltaic applications^{8,9}. Due to its inherent transparency in the visible range, ZnO is used as transparent conductive oxide (TCO) on top of thin film solar cell^{10,11}. As an example, in inverted bulk-heterojunction organic solar cells^{12,13}, *n*-doped ZnO can be used as the electron collector/hole blocking buffer layer¹⁴.

ZnO thin films can be either deposited¹⁵ or solution processed¹⁴. Determination of the doping concentration of ZnO films is a fundamental step for finely tuning ZnO deposition parameters (e.g. for epitaxial growth) and ZnO nanoparticles synthesis (for solution processing). A method able to determine thin films ZnO doping profiles at the nanoscale would allow optimizing its performance in several applications.

Although different techniques to measure the doping concentration in semiconductors have been developed^{16–18}, the determination of this property in ZnO thin films still remains challenging¹⁹. This is due to the fact that ZnO is intrinsically *n*-doped, presumably by Zn interstitials, O vacancies and H, that affect the position of the Fermi level within the bandgap²⁰. In this view, ordinary method such as Secondary Ion-Mass Spectroscopy (SIMS) and Electron Holography (EH) can just give an insight of the possible cause of the self-doping effect^{21,22}, without giving accurate quantitative results in terms of charge carrier concentration. Furthermore, these two techniques are destructive and therefore their versatility is limited. Four Probe Method is the most widespread technique to measure the resistivity of thin films²³. From this measurement, given the carriers mobility, the effective doping concentration of the material can be recovered. However, several experimental issues have to be taken into account when using this technique. The contact between a metal and a semiconductor can form a Schottky diode²⁴ rather than an ohmic contact. To obtain reliable results, adjustments of the drive current are needed depending of the resistivity of the sample. Due to the reduced thickness of thin films, the measurement can be affected by the presence of the substrate, leading to erroneous results. In this view, a



non-contact technique able to measure the position of the Fermi level and to relate it with the effective doping concentration would represent an adequate solution for the aforementioned issues.

Scanning Kelvin Probe Microscopy (SKPM), a modified version of Atomic Force Microscopy (AFM), is a non-destructive non-contact surface technique that allows imaging two-dimensional profiles of contact potential difference (V_{CPD}) i.e. the difference in the work functions of the tip and the sample^{25–28}. This is true in absence of trapped charges²⁹ or adsorbates on the surface. It is well known that in semiconductors the work function depends on the dopant types and concentrations²⁴. This is because they affect the Fermi level position within the bandgap.

Different attempts to correlate SKPM measurements with doping concentration in semiconductors have been reported in literature since the technique has been proposed^{27,30}. Henning³¹, Shin³² and Hochwitz³³ reported a doping concentration two-dimensional image in silicon microstructures and integrated circuits. Due to its inherent nanometric spatial resolution²⁹, SKPM has been successively used to probe non-uniform doping distribution at the nanoscale. Semenikhin³⁴ reported evidence of local doping inhomogeneity on conducting polybithiophene, while Koren³⁵ measured the doping distribution along single phosphorous-doped silicon nanowires. Although compared with Scanning Capacitance Microscopy (SCP) this technique presents some limitations in terms of accuracy^{36,37}, previously mentioned and other reports³⁸ demonstrate that SKPM can be used to quantitatively measure the doping concentration in semiconductors with high spatial resolution^{31,33,39}. Attempts to correlate SKPM measurements with charge carriers concentration in ZnO have been reported^{40,41}. However, a clear and complete formalism is still lacking.

Measuring the doping concentration of a sample without touching its surface represents a considerable advantage, especially for thin films. This avoids damaging the surface and does not introduce extra effects due to Schottky barrier formation. Compared to Four Probe Method, SKPM can be used to measure the doping profile of semiconducting thin films deposited on metal⁴¹. This would prevent from the need to deposit a sample on an insulating substrate just to measure its resistivity. Being a surface technique, SKPM is able to measure carrier concentration on top of the sample. Here, the presence of charges can affect the measurement. To minimize this effect, the sample is scanned in tapping mode while both the tip and the back contact are connected to the ground, before performing the actual experiments. By creating a closed circuit, the surface charges flows towards the electric ground, causing the surface to discharge. This technique has been successfully applied by Jespersen et al.⁴². While doping concentration is normally associated with bulk intrinsic or extrinsic doping, due to their small thickness, surface defects in thin

films have a significant contribution on the overall sample doping⁴³. This has been experimentally demonstrated by photovoltage measurements performed on ZnO nano-“mounds”⁴⁴. Since SKPM is able to measure the presence of surface defects⁴⁵, it represents a suitable technique for imaging two-dimensional doping concentration in ZnO thin films.

In this paper, two-dimensional charge carrier concentration images acquired on RF-sputtered intrinsic ZnO thin films are reported. A simple energy band model that correlates work function difference measurements with the effective doping concentration is presented. ZnO samples with different thickness (from 10 to 300 nm) are investigated. To further validate the method, doping concentrations of ZnO samples deposited under different conditions are compared. We show that results inferred with this technique are in accordance with carrier concentration obtained with Four Probe and Hall measurements.

SKPM is an AFM based technique developed by Nonnemacher et al. in 1991^{27,30}. As other electrostatic force microscopy techniques^{39,46}, it measures the contact potential difference V_{CPD} between a conductive tip and a sample. The V_{CPD} is defined as:

$$V_{CPD} = \frac{\phi_{tip} - \phi_{sample}}{q} \quad (1)$$

where q is the electronic charge, while ϕ_{tip} and ϕ_{sample} are the work functions of the tip and the sample respectively. Compared to Ultraviolet Photoelectron Spectroscopy (UPS), which measures the kinetic energy of spectra of photoelectrons emitted under ultraviolet excitation, both techniques can be used to quantify the work function of a given material and therefore could be employed to determine the charge carrier concentration. However, UPS has a lower spatial resolution compared to SKPM, being limited by the dimension of the ultraviolet light spot used as excitation⁴⁷. Thus, in order to quantify the charge carrier concentration with high spatial resolution, we rely on SKPM. In SKPM, when the tip is brought close to the sample and they are both grounded, an electrostatic interaction due to the differences in their Fermi energy levels can be probed. Fig. 1 shows the energy level diagram of the tip and the sample for different ϕ_{tip} and ϕ_{sample} . When tip and sample are not electrically connected, their vacuum levels are aligned but Fermi energy levels are different (Fig. 1a). Upon electrical contact (for example both grounded), the system reaches equilibrium, and Fermi levels line-up through electron current flow (Fig. 1b). This current flow causes the vacuum energy levels to be no longer the same: the consequence of this is the formation of a contact potential difference V_{CPD} that affects the interaction between the tip and the sample, causing the formation of an electrostatic force between them. As shown in Fig. 1c, this force

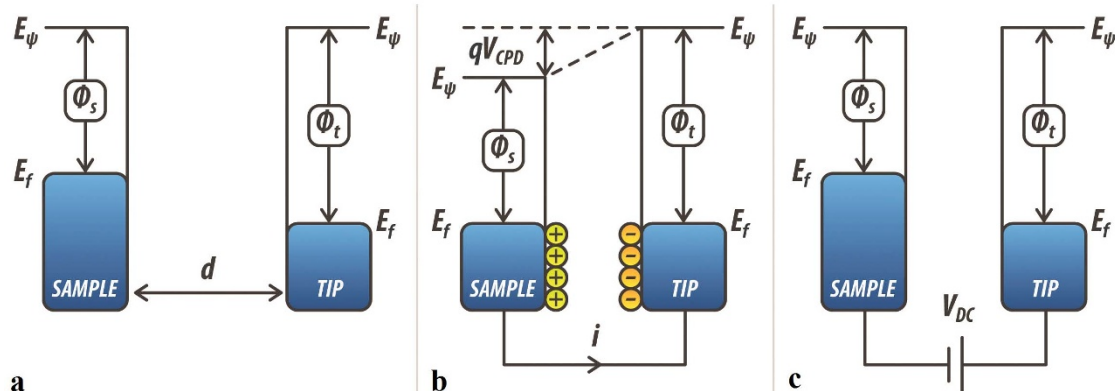


Figure 1 | Electronic energy levels of the tip-sample system for three different cases. (a) tip and sample are separated by a distance d and are not electrically connected; (b) tip and sample are electrically connected. In this case the Fermi energy levels are lined-up; (c) an external bias equal to the contact potential difference V_{CPD} is applied to the tip. This causes the tip-sample electrical force to be nullified.



can be nullified. This is done indeed applying an external bias $V_{DC} = V_{CPD}$ between the tip and the sample. Thus, in this case, the amount of applied external bias is exactly equal to the work function difference between the two.

In SKPM the contact potential difference V_{CPD} between a conductive tip and a sample is measured by applying to the tip an ac voltage ($V_{ac} = V_{AC}\sin(\omega t)$) and a dc voltage (V_{DC}). The V_{ac} causes the cantilever to oscillate because of the electrical forces between the AFM tip and the sample surface, while the V_{DC} nullifies the oscillating electrical forces that originated from the V_{CPD} . The frequency ω is chosen equal or close to the resonance frequency of the cantilever in order to increase the signal-to-noise ratio. The electrostatic force component measured at frequency ω has the following expression^{27,30,32}:

$$F_{\omega} = -\frac{dC}{dz}(V_{DC} - V_{CPD})V_{AC}\sin(\omega t) \quad (2)$$

where C is the tip-sample capacitance and z is the tip-sample distance. From (2), it is evident that the V_{CPD} can be measured by applying a dc voltage V_{DC} such that the oscillating amplitude at ω is nullified. Equation (2) is strictly valid for metallic samples. However, it has been demonstrated that a similar expression can be derived for semiconductors, provided that the tip-sample capacitance is written as the sum of the air gap and the space-charge capacitor⁴⁸.

The Fermi energy level in semiconductors depends on the doping concentration²⁴. Fig. 2 depicts the electronic energy level for a tip-semiconductor system when the tip and the back surface of the semiconductor are electrically connected. In the case of a non-degenerate n -doped semiconductor, the Boltzmann approximation for the concentration of electrons (n) reads⁴⁹:

$$n = N_c \exp\left(\frac{E_F - E_c}{K_B T}\right) \quad (3)$$

where N_c is the effective density of states in the conduction band, E_c and E_F are the conduction band energy level and the Fermi energy level, K_B is Boltzmann constant and T is the temperature. If the effective donors concentration C_D is significantly higher than the intrinsic carriers concentrations n_i , the concentration of electrons n can be used to estimate C_D by using the following approximation⁴⁹:

$$C_D \stackrel{\text{def}}{=} N_D^+ - N_A^- \approx n \quad (4)$$

where the effective donors concentration C_D is defined as the difference between the ionized concentration of donors N_D^+ and the ionized concentration of acceptors N_A^- . When the n -doped semiconductor surface is electrically connected to the tip through a back contact, the V_{CPD} can be written as³²:

$$V_{CPD} = \frac{\phi_{tip} - \chi + (E_F - E_c)}{q} \quad (5)$$

where χ is the electron affinity of the semiconductor. Analogous expressions can be derived for a p -doped semiconducting surface. In equation (5) the band bending term ϕ_B is not explicitly included and its effect on the electrical conductivity of the surface is taken into account by including it in the bulk. Due to their limited thickness, indeed, we expect the presence of defect states at the surface to affect the charge carrier concentration through the entire film. This assumption is supported by Ref. 44, where photovoltage measurements confirm the presence of electrically-active deep levels due to zinc vacancies that affects the surface potential on a scale of hundreds of nanometers.

Finally, by combining equations (3–5), V_{CPD} images probed by SKPM can be mapped into the effective donors concentration C_D , which actually corresponds to the effective doping profile:

$$C_D \approx N_c \exp\left(\frac{qV_{CPD} - \phi_{tip} + \chi}{K_B T}\right) \quad (6)$$

While performing SKPM scans, two main sources of errors must be taken into account: stray capacitances from tip geometry, and environmentally mediated water layers presence³². In the ideal case, it is generally assumed that the tip-sample capacitance is essentially due to the effect of the tip apex³². However, the contribution from the tip cone and the cantilever can be significant^{37,50}. Therefore, it is possible that measured SKPM values differ from theoretical ones. Gil et al.⁵¹ reported that the standard interpretation of data may be incorrect because the total force is produced not only by the end of the tip, but also by the contributions of the cantilever and the tip cone, which senses a different surface potential than the tip. Jacobs et al.⁵² demonstrated that reasonable V_{CPD} values can only be obtained by using tips with a long cone and by reducing the lift height during the SKPM interleave scan. In the present work, tips with a long cone (tip height $14 \pm 4 \mu\text{m}$) and a small tip angle (15 ± 5 degrees) are employed. Moreover, the surface is scanned at a small tip-sample distance (20 nm). This allows minimizing the effect of the tip cone and the lever, which would dominate instead at larger tip-sample separations. We have quantified indeed that at 20 nm away from the surface, for our cantilever (ASYELEC 0.1) the tip contributes to more than 50% of the total electrostatic interaction and its contribution is therefore the most relevant among all. The contributions of the cone and the lever can be further reduced by measuring the gradient of the force instead of the force itself⁵³. Furthermore, scanning at small tip-sample separations allows maintaining a high spatial resolution because the smaller is the distance, the smaller is the area of interaction of the AFM probe⁵⁴. A small oscillating amplitude (5 nm) is used in this case to maintain the system working in the harmonic

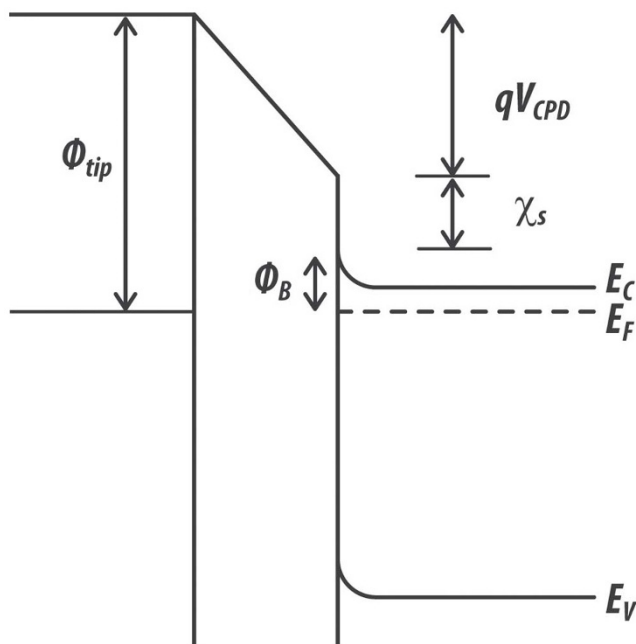


Figure 2 | Electronic energy band line-up for a metallic tip-semiconductor system when the tip and the back surface of the semiconductor are electrically connected. The contact potential difference V_{CPD} depends on the tip work function ϕ_{tip} , on the electron affinity of the semiconductor χ , as well as on the difference between the bottom energy level of the conduction band E_c and the Fermi level E_F in the semiconductor. In this case, the effect of the surface band bending ϕ_B is included in the bulk.

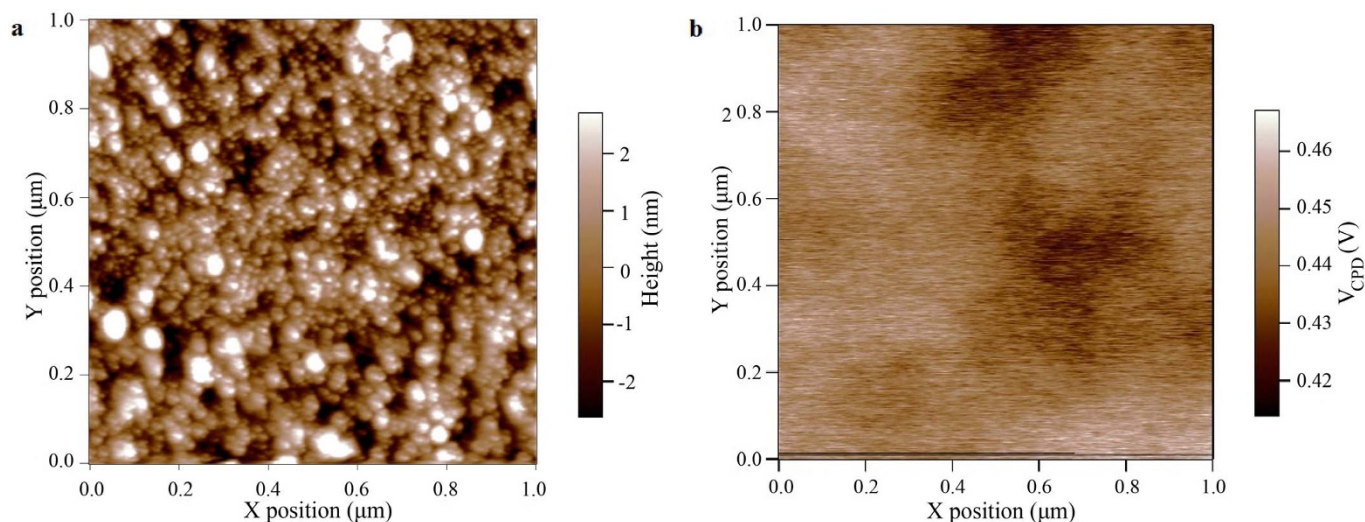


Figure 3 | (a) Atomic force microscopy topography image of a ZnO thin film deposited by RF sputtering. Small grains with dimensions of tens of nanometers can be observed (b) Two-dimensional contact potential difference V_{CPD} image of the same surface imaged in Fig. 3a. The image is acquired at an equilibrium distance of 20 nm with an oscillation of 5 nm.

regime. This has been verified by looking at the shape of the electrical tuning where no distortions in the Lorentzian function (amplitude vs. frequency) were observed. When a high value of V_{AC} is employed, the tuning curve may present distortions, causing bi-stability in the tip-sample interaction⁵⁵. Another source of inaccuracy in the measurement of V_{CPD} is the presence of water layers or molecular adsorbates on the sample surface. It has been shown that the presence of a thin layer of water or water vapor in the environment can cause deviations in the measurement of the resistivity of metal-oxide films⁵⁶. Water molecules are generally chemisorbed and physisorbed by the surface⁵⁷, and this process increases or decreases the surface electron conductivity depending on the type of the semiconductor (respectively n or p type)⁵⁸. In the present work, we minimize the effect of water layers and adsorbates by preparing the samples by cycles of Ar^+ bombardment at 250°C, followed by annealing at 120°C in a vacuum chamber. Samples are transferred from the sputtering chamber to the AFM in an environmental chamber filled with N_2 in order to minimize the exposure to humidity and SKPM measurements are performed in dry and inert atmosphere (N_2 , relative humidity < 10%).

Results

The experiment consists of three steps. First of all, the back metal (Ag) is connected to the electrical ground and a SKPM scan is performed on top of metal surface (a portion of back metal surface is intentionally not covered with ZnO for this purpose). This is done to measure the metal work function. A calibrated tip (with known work function) is used for this purpose. Depending on the specific sample, small changes in value (± 0.1 eV) have been measured. No dependency of Ag work function on relative humidity was found. After that, the same procedure is repeated with another tip in order to measure its work function. By doing so, we are able to calibrate each tip. Secondly, the tip is connected to the ground and the top surface of the ZnO sample is scanned in tapping mode. As previously mentioned, this procedure is done in order to discharge the surface before starting the SKPM measurement. Finally, the same portion of the surface is scanned with SKPM. A positive ac voltage V_{ac} is applied to the tip. In this case, electrons (majority carriers in n -doped semiconductors) are attracted to the top surface of the sample. Thus, the semiconductor is in the accumulation regime and the metal/semiconductor system can be treated in a first approximation as a metal/metal system, allowing for the determination of the V_{CPD} ⁴⁸.

Before starting the experiments on ZnO, SKPM measurements are carried out on silicon and germanium samples with known charge carrier concentration. This is done to validate the model. Samples are etched with HF in order to remove their native oxide. Doping concentrations in accordance with nominal values are recovered, confirming the reliability of this technique. After that, the same experiments are performed on ZnO.

An AFM topography image of the surface of a ZnO thin film with the corresponding contact potential V_{CPD} image, acquired at a distance of 20 nm, is shown in Fig. 3. Fig. 3a shows the typical polycrystalline nature of ZnO sputtered thin film, with small grains of nanometric dimension (tens of nanometers). The contact potential V_{CPD} image in Fig. 3b does not show the same morphological features reported in Fig. 3a. The V_{CPD} value appears almost uniform, varying within 10% of the mean value. Similar V_{CPD} values with a deviation in the order of 5% are recorded after scanning the same portion of the surface for more than 1 hour. This result confirms that no charging phenomena are taking place. The same experiment was repeated one week after the first measurement, keeping in the meanwhile the sample in inert atmosphere. No sensible variation in the V_{CPD} was measured.

In order to relate the V_{CPD} with the effective doping concentration of thin film ZnO, all the parameters in equation (6) have to be recovered. In Table 1, the value of N_C and χ for room temperature RF sputtered ZnO as well as the value of ϕ for Ag are reported. While the first two are taken from¹⁹, the value of ϕ for Ag is measured for each sample as previously pointed out.

As long as the sample temperature is kept constant, these parameters do not change with thickness and deposition conditions⁵⁹. Fig. 4a shows a two-dimensional map of the effective doping concentration in a 150 nm thick ZnO layer. In Fig. 4b the charge carrier

Table 1 | ZnO and Ag parameters extracted from experimental results

Quantity	Value and Reference
ZnO effective density of states in the conduction band N_C	$3.7 \cdot 10^{18} \text{ cm}^{-3}$ ¹⁹
ZnO electron affinity χ	4.5 eV ¹⁹
Ag work function ϕ	4.7 ± 0.1 V

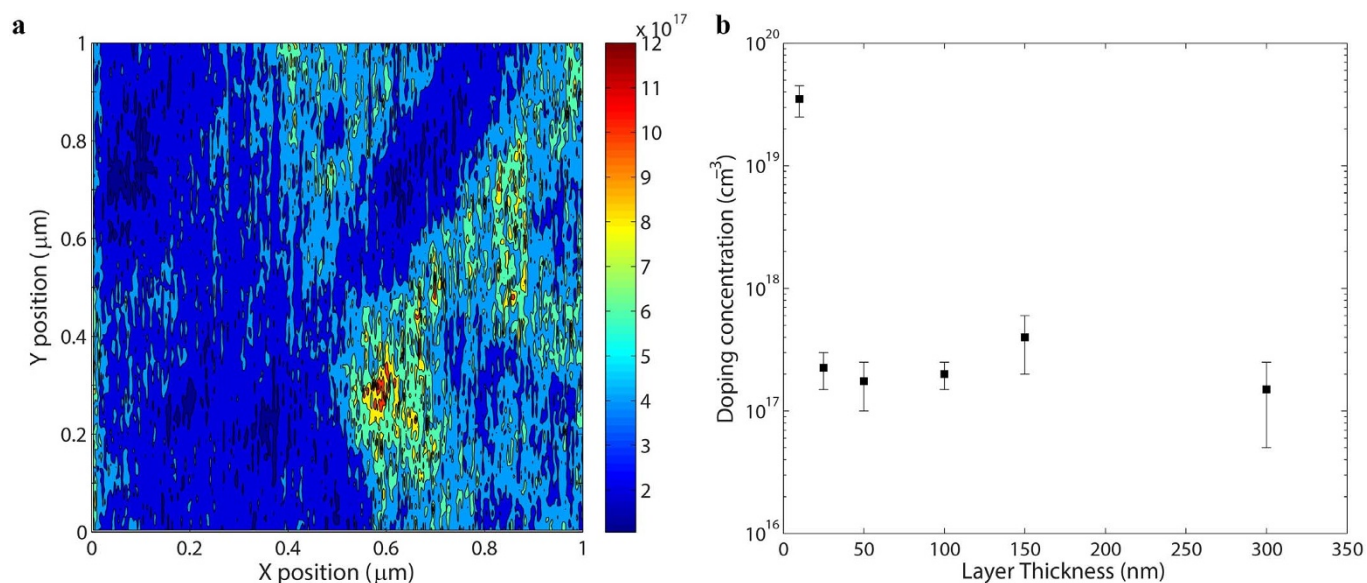


Figure 4 | (a) Two-dimensional map of the charge carrier density in a 150 nm thick ZnO film. (b) doping concentration versus layer thickness for a set of ZnO thin films (from 10 to 300 nm). All the samples are deposited under the same conditions (deposition rate 0.1 Å/sec, Ar pressure 0.8 mTorr). The effective doping concentration does not correlate with the layer thickness, except for the 10 nm layer. For each sample, three different regions have been scanned. The standard deviation of the value of the effective doping concentration is reported.

density is plotted versus the layer thickness (from 10 to 300 nm). Each sample is deposited under the same conditions (deposition rate 0.1 Å/sec, Ar pressure 0.8 mTorr). The average value as well as the standard deviation of the contact potential difference V_{CPD} measured on all the samples is reported in the supplementary material. The uncertainty in the quantification of the free carrier concentration of this technique is given by the calibration process i.e. the quantification of the V_{CPD} between the tip and the Ag surface.

Doping concentrations in the order of 10^{17} cm⁻³ are recovered for all the samples. This value is in agreement with Four Probe measurements

performed on polycrystalline ZnO samples deposited under the same conditions on an insulating substrate (resistivity $\rho = 0.7\text{--}1.8$ Ωcm, which, given a measured electron mobility of 31 ± 3 cm²/Vs, gives a doping concentration of $\sim 1 \cdot 10^{17}\text{--}3 \cdot 10^{17}$ cm⁻³). Furthermore, the doping concentration does not correlate with layer thickness. This is valid for layers with a thickness larger than the electron mean free path in ZnO (close to 20 nm)⁶⁰. Below this limit, the proposed model is not valid since quantum effects become relevant and the transport regime is not diffusive anymore⁶¹. Therefore it cannot be applied to quantify the doping concentration in the material.

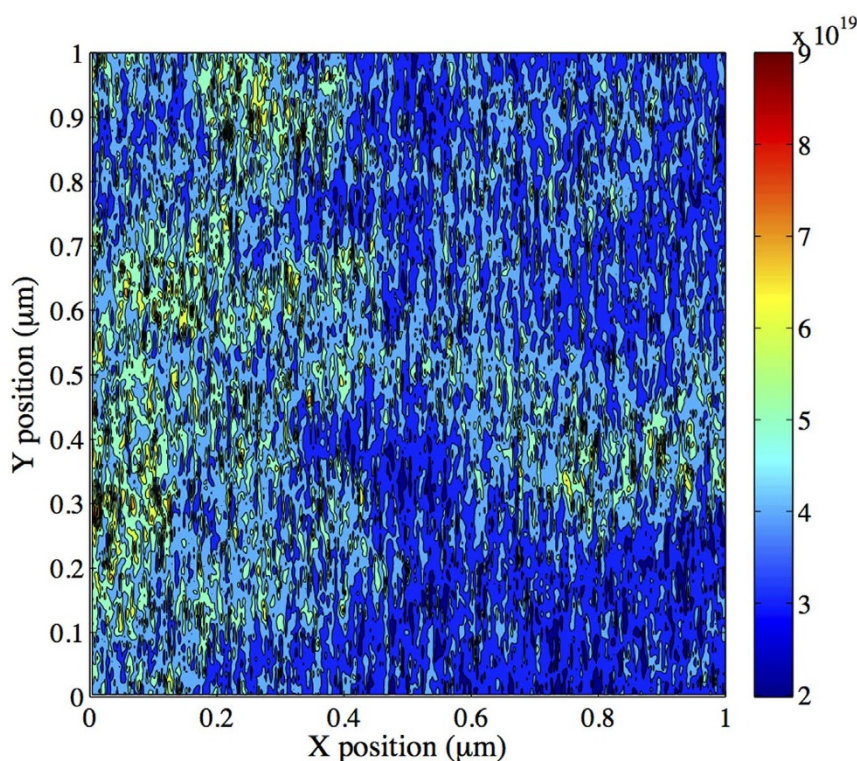


Figure 5 | Two-dimensional map of the charge carrier density in ZnO thin film (thickness 100 nm, deposition rate 0.2 Å/sec, Ar pressure 10 mTorr).



In order to further validate the technique, a thin film ZnO with a thickness of 100 nm, deposited with a higher deposition rate (0.2 Å/sec) and with higher Ar pressure (10 mTorr), is measured. It has been experimentally demonstrated that an increase in the deposition rate as well as in the Ar pressure causes the doping carrier concentration in ZnO thin films to increase⁶². In this case, we measure an increase in the work function difference (approximately 200 mV, from an average value of 445 mV to 647 mV) between the metal and the ZnO with respect to the previous case. This difference is attributed to a change in the charge carrier concentration because no considerable difference in mean surface roughness (from 4 to 4.2 nm) as well as in electron mobility (from 31 to 40 cm²/Vs) was measured. Fig. 5 shows the sample charge concentration image. An average charge carrier density in the order of 10¹⁹ cm⁻³ is calculated. Therefore, an increase of two orders of magnitude in the doping concentration is achieved by changing the deposition parameters. Being in accordance with experimental results reported in literature⁶² and with our Four Probe measurements ($\rho = 0.9 \cdot 10^{-2} \Omega \cdot \text{cm}$), these results confirm the ability of the technique to measure the doping concentration of ZnO thin layers deposited under different conditions.

Conclusions

We probed the charge carrier density in ZnO thin films with high spatial resolution by using SKPM. A simple electronic energy model is used to correlate the work function of the sample with the effective doping concentration in the ZnO thin films. Limitations of this technique (stray capacitances from tip geometry, water layer presence, surface charges and adsorbates) are discussed and possible solutions are proposed. The technique is experimentally tested on a set of samples deposited by RF sputtering under different conditions. Finally, we showed that results inferred with this technique are in accordance with carrier concentration expected for intrinsic ZnO thin films deposited with two different deposition rate and Ar pressure and obtained with Four Probe and Hall measurements.

Methods

SKPM measurements are performed on ZnO layers deposited by Radio Frequency (RF) sputtering on top of Ag. A set of samples with different thickness (from 10 to 300 nm approximately) is analyzed. The samples are deposited and their surface is pretreated (Ar⁺ bombardment at 250°C), annealed at 120°C in a vacuum chamber and immediately measured. SKPM measurements are performed in inert atmosphere (N₂) with a Cypher (Asylum Research, USA). A Si cantilever coated with Ti-Ir (ASYLEC-01) is used. A cantilever resonant frequency ω_0 of ~71 KHz, Q factor of 130 and a spring constant k of 1.5 N/m were measured using a thermal noise method⁶³.

The average value as well as the standard deviation of the contact potential difference V_{CPD} measured on all thin film ZnO samples are reported in the supporting information.

- Duan, L. *et al.* Stable p-type ZnO films dual-doped with silver and nitrogen. *Solid State Commun.* **157**, 45–48 (2013).
- Zhang, Y., Guo, T., Luo, Y. D., Lin, Y. H. & Nan, C. W. Tunable Ferromagnetic Behaviors Observed in Highly Orientated Co-Doped ZnO Thin Films by the Bandgap Engineering. *J. Am. Ceram. Soc.* **96**, 361–364 (2013).
- Kim, Y. H. *et al.* Realizing the Potential of ZnO with Alternative Non-Metallic Co-Dopants as Electrode Materials for Small Molecule Optoelectronic Devices. *Adv. Funct. Mater.* **23**, 3645–3652 (2013).
- Dodds, J. S., Meyers, F. N. & Loh, K. J. Piezoelectric characterization of PVDF-TrFE thin films enhanced with ZnO nanoparticles. *Sens. Journ., IEEE* **12**, 1889–1890 (2012).
- Pearton, S. J. *et al.* ZnO spintronics and nanowire devices. *J. Electron. Mater.* **35**, 862–868, doi:10.1007/bf02692541 (2006).
- Ozgun, U., Hofstetter, D. & Morkoc, H. ZnO Devices and Applications: A Review of Current Status and Future Prospects. *Proceed. of the IEEE* **98**, 1255–1268, doi:10.1109/jproc.2010.2044550 (2010).
- McGlynn, E. ZnO Nanostructures and Their Applications. *Contemp. Phys.* 1–2, doi:10.1080/00107514.2013.776113 (2013).
- Nagata, T. *et al.* Photoelectron spectroscopic study of band alignment of polymer/ZnO photovoltaic device structure. *Appl. Phys. Lett.* **102**, 043302–043302-043304 (2013).
- Maragliano, C., Stefancich, M., Rampino, S. & Colace, L. Realistic simulation of polycrystalline CIGS absorbers and experimental verification. *MRS Online Proceedings Library* **1493**, doi:10.1557/opl.2013.401 (2013).
- Repins, I. *et al.* 19.9%-efficient ZnO/CdS/CuInGaSe₂ solar cell with 81.2% fill factor. *Progr. in Photov.: Research and Applications* **16**, 235–239, doi:10.1002/pip.822 (2008).
- Maragliano, C., Colace, L., Chiesa, M., Rampino, S. & Stefancich, M. Three-Dimensional Cu(InGa)Se₂ Photovoltaic Cells Simulations: Optimization for Limited-Range Wavelength Applications. *IEEE Journ. of Photov.* doi:http://dx.doi.org/10.1109/JPHOTOV.2013.2258191 (2013).
- Lilliu, S. *et al.* Dynamics of crystallization and disorder during annealing of P3HT/PCBM bulk heterojunctions. *Macromolecules* **44**, 2725–2734 (2011).
- Krebs, F. C. Fabrication and processing of polymer solar cells: A review of printing and coating techniques. *Sol. Energy Mater. Sol. Cells* **93**, 394–412, doi:http://dx.doi.org/10.1016/j.solmat.2008.10.004 (2009).
- Huang, J., Yin, Z. & Zheng, Q. Applications of ZnO in organic and hybrid solar cells. *Energy & Environm. Science* **4**, 3861–3877 (2011).
- Xu, W. *et al.* Low-pressure MOCVD growth of p-type ZnO thin films by using NO as the dopant source. *Journ. of Crystal Growth* **265**, 133–136, doi:http://dx.doi.org/10.1016/j.jcrysgro.2003.12.061 (2004).
- Ellmer, K. in *Characterization of Materials* (John Wiley & Sons, Inc., 2002).
- Vickerman, J. C. Secondary ion mass spectrometry—basic concepts, instrumental aspects, applications and trends (Wiley, New York, 1987).
- Rau, W., Schwander, P., Baumann, F., Höppner, W. & Ourmazd, A. Two-dimensional mapping of the electrostatic potential in transistors by electron holography. *Phys. Rev. Lett.* **82**, 2614–2617 (1999).
- Ellmer, K. [*Transparent Conductive Zinc Oxide*] *Springer Series in Materials Science* (Springer Berlin Heidelberg, 2008).
- Coleman, V. A. & Jagadish, C. *Zinc Oxide Bulk, Thin Films and Nanostructures* (Elsevier Science Ltd, 2006).
- Saw, K. G., Ibrahim, K., Lim, Y. T. & Chai, M. K. Self-compensation in ZnO thin films: An insight from X-ray photoelectron spectroscopy, Raman spectroscopy and time-of-flight secondary ion mass spectroscopy analyses. *Thin Solid Films* **515**, 2879–2884, doi:http://dx.doi.org/10.1016/j.tsf.2006.08.047 (2007).
- Müller, E. *et al.* Probing the electrostatic potential of charged dislocations in n-GaN and n-ZnO epilayers by transmission electron holography. *Phys. Rev. B* **73**, 245316 (2006).
- Schuisly, M., Elam, J. W. & George, S. M. In situ resistivity measurements during the atomic layer deposition of ZnO and W thin films. *Appl. Phys. Lett.* **81**, 180–182 (2002).
- Sze, S. M. & Ng, K. K. *Physics of semiconductor devices.* (Wiley-interscience, 2006).
- Melitz, W., Shen, J., Kummel, A. C. & Lee, S. Kelvin probe force microscopy and its application. *Surf. Sci. Rep.* **66**, 1–27, doi:http://dx.doi.org/10.1016/j.surfrep.2010.10.001 (2011).
- Nonnenmacher, M., O'Boyle, M. P. & Wickramasinghe, H. K. Kelvin probe force microscopy. *Applied Physics Letters* **58**, 2921–2923 (1991).
- Nonnenmacher, M., O'Boyle, M. & Wickramasinghe, H. K. Surface investigations with a Kelvin probe force microscope. *Ultramicroscopy* **42–44**, 268–273, doi:10.1016/0304-3991(92)90278-r (1992).
- Girard, P. Electrostatic force microscopy: principles and some applications to semiconductors. *Nanotechnology* **12** (2001).
- Zerweck, U., Loppacher, C., Otto, T., Grafström, S. & Eng, L. M. Accuracy and resolution limits of Kelvin probe force microscopy. *Phys. Rev. B* **71**, 125424 (2005).
- Nonnenmacher, M., O'Boyle, M. P. & Wickramasinghe, H. K. Kelvin probe force microscopy. *Appl. Phys. Lett.* **58**, 2921–2923, doi:10.1063/1.105227 (1991).
- Henning, A. K. *et al.* Two dimensional surface dopant profiling in silicon using scanning Kelvin probe microscopy. *J. Appl. Phys.* **77**, 1888–1896, doi:10.1063/1.358819 (1995).
- Shin, H. *et al.* Measurement and Visualization of Doping Profile in Silicon Using Kelvin Probe Force Microscopy (KPFM). *Electronic Mat. Lett.* **1**, 127–133 (2005).
- Hochwitz, T. *et al.* Imaging integrated circuit dopant profiles with the force-based scanning Kelvin probe microscope. *Journal of Vacuum Science & Tech. B: Microel. and Nanometer Struct.* **14**, 440–446, doi:10.1116/1.588491 (1996).
- Semenikhin, O. A., Jiang, L., Iyoda, T., Hashimoto, K. & Fujishima, A. Atomic Force Microscopy and Kelvin Probe Force Microscopy Evidence of Local Structural Inhomogeneity and Nonuniform Dopant Distribution in Conducting Poly(bithiophene). *The Journ. Phys. Chem.* **100**, 18603–18606, doi:10.1021/jp960844y (1996).
- Koren, E., Rosenwaks, Y., Allen, J. E., Hemesath, E. R. & Lauhon, L. J. Nonuniform doping distribution along silicon nanowires measured by Kelvin probe force microscopy and scanning photocurrent microscopy. *Appl. Phys. Lett.* **95**, 092105–092105-092103, doi:10.1063/1.3207887 (2009).
- Park, S.-E., Nguyen, N. V., Kopanski, J. J., Suehle, J. S. & Vogel, E. M. Comparison of scanning capacitance microscopy and scanning Kelvin probe microscopy in determining two-dimensional doping profiles of Si homostructures. *J. Vac. Sci. Technol. B* **24**, 404, doi:http://dx.doi.org/10.1116/1.2162569 (2006).
- Koley, G., Spencer, M. G. & Bhangale, H. R. Cantilever effects on the measurement of electrostatic potentials by scanning Kelvin probe microscopy. *Appl. Phys. Lett.* **79**, 545–547 (2001).
- Koren, E. *et al.* Obtaining Uniform Dopant Distributions in VLS-Grown Si Nanowires. *Nano Lett.* **11**, 183–187, doi:10.1021/nl103363c (2010).



39. Maragliano, C., Heskes, D., Stefancich, M., Chiesa, M. & Souier, T. Dynamic electrostatic force microscopy technique for the study of electrical properties with improved spatial resolution. *Nanotechnology* **24**, 225703 (2013).
40. Van Ben, C., Cho, H. D., Kang, T. W. & Yang, W. Doping transition of doped ZnO nanorods measured by Kelvin probe force microscopy. *Thin Solid Films* **520**, 4622–4625, doi:http://dx.doi.org/10.1016/j.tsf.2011.10.129 (2012).
41. Lakhwani, G. *et al.* Probing Charge Carrier Density in a Layer of Photodoped ZnO Nanoparticles by Spectroscopic Ellipsometry. *The Journ. of Phys. Chem. C* **114**, 14804–14810, doi:10.1021/jp104846h (2010).
42. Jespersen, T. S. & Nygård, J. Charge Trapping in Carbon Nanotube Loops Demonstrated by Electrostatic Force Microscopy. *Nano Lett.* **5**, 1838–1841, doi:10.1021/nl0505997 (2005).
43. Ohring, M. *Materials science of thin films.* (Academic press, 2001).
44. Merz, T. A., Doust, D. R., Bolton, T., Dong, Y. & Brillson, L. J. Nanostructure growth-induced defect formation and band bending at ZnO surfaces. *Surf. Sci.* **605**, L20–L23, doi:http://dx.doi.org/10.1016/j.susc.2010.12.021 (2011).
45. Rosenwaks, Y., Shikler, R., Glatzel, T. & Sadewasser, S. Kelvin probe force microscopy of semiconductor surface defects. *Phys. Rev. B* **70**, 085320 (2004).
46. Lilliu, S. *et al.* EFM data mapped into 2D images of tip sample potential difference and capacitance second derivative. *Nat. Scient. Rep.* (2013).
47. Rabalais, J. W. & Rabalais, J. W. *Principles of ultraviolet photoelectron spectroscopy.* (Wiley New York, 1977).
48. Hudlet, S., Saint Jean, M., Roulet, B., Berger, J. & Guthmann, C. Electrostatic forces between metallic tip and semiconductor surfaces. *J. Appl. Phys.* **77**, 3308–3314, doi:10.1063/1.358616 (1995).
49. Sze, S. M. & Kwok, K. N. *Physics of Semiconductor Devices.* Third edn, (Wiley-interscience, 2007).
50. Gómez-Moñivas, S., Froufe, L. S., Carminati, R., Greffet, J. J. & Sáenz, J. J. Tip-shape effects on electrostatic force microscopy resolution. *Nanotechnology* **12**, 496 (2001).
51. Gil, A., Colchero, J., Gómez-Herrero, J. & Baró, A. M. Electrostatic force gradient signal: resolution enhancement in electrostatic force microscopy and improved Kelvin probe microscopy. *Nanotechnology* **14**, 332 (2003).
52. Jacobs, H. O., Leuchtmann, P., Homan, O. J. & Stemmer, A. Resolution and contrast in Kelvin probe force microscopy. *J. Appl. Phys.* **84**, 1168–1173 (1998).
53. Colchero, J., Gil, A. & Baró, A. M. Resolution enhancement and improved data interpretation in electrostatic force microscopy. *Phys. Rev. B* **64**, 245403 (2001).
54. Santos, S. *et al.* How localized are energy dissipation processes in nanoscale interactions? *Nanotechnology* **22**, 345401 (2011).
55. San Paulo, A. & Garcia, R. Unifying theory of tapping-mode atomic-force microscopy. *Phys. Rev. B* **66**, 041406 (2002).
56. Dixit, S., Srivastava, A., Shukla, R. K. & Srivastava, A. Pulsed laser deposited ZnO films and their humidity sensing behavior. *J. Mater. Sci.: Mater. Electron.* **19**, 788–792, doi:10.1007/s10854-007-9414-2 (2008).
57. Cox, P. *The surface science of metal oxides.* (Cambridge university press, 1996).
58. Seiyama, T., Yamazoe, N. & Arai, H. Ceramic humidity sensors. *Sensors and Actuators* **4**, 85–96, doi:http://dx.doi.org/10.1016/0250-6874(83)85012-4 (1983).
59. Jacobi, K., Zwicker, G. & Gutmann, A. Work function, electron affinity and band bending of zinc oxide surfaces. *Surf. Sci.* **141**, 109–125, doi:http://dx.doi.org/10.1016/0039-6028(84)90199-7 (1984).
60. Baxter, J. B. & Schmuttenmaer, C. A. Conductivity of ZnO nanowires, nanoparticles, and thin films using time-resolved terahertz spectroscopy. *The Journ. Phys. Chem. B* **110**, 25229–25239 (2006).
61. Alkhatib, A., Souier, T. & Chiesa, M. Morphology dependent electrical transport behavior in gold nanostructures. *Thin Solid Films* **520**, 656–661 (2011).
62. Gao, W. & Li, Z. ZnO thin films produced by magnetron sputtering. *Ceram. Int.* **30**, 1155–1159, doi:http://dx.doi.org/10.1016/j.ceramint.2003.12.197 (2004).
63. Hutter, J. L. & Bechhoefer, J. Calibration of atomic-force microscope tips. *Rev. Sci. Instrum.* **64**, 1868–1873 (1993).

Acknowledgments

We thank Yamila Omar for proofreading the manuscript.

Author contributions

C.M. and S.L. developed the technique, conducted the experiments, prepared the figures and wrote the manuscript. M.S.D., M.C. and M.S. supervised the project. T.S. and M.S. helped with the theoretical development of the technique.

Additional information

Supplementary information accompanies this paper at <http://www.nature.com/scientificreports>

Competing financial interests: The authors declare no competing financial interests.

How to cite this article: Maragliano, C. *et al.* Quantifying charge carrier concentration in ZnO thin films by Scanning Kelvin Probe Microscopy. *Sci. Rep.* **4**, 4203; DOI:10.1038/srep04203 (2014).



This work is licensed under a Creative Commons Attribution-NonCommercial-NoDerivs 3.0 Unported license. To view a copy of this license, visit <http://creativecommons.org/licenses/by-nc-nd/3.0>